



Toward Standardization of Electrophysiology and Computational Tissue Strain in Rodent Intracortical Microelectrode Models

OPEN ACCESS

Edited by:

Senentxu Lanceros-Mendez,
Basque Center for Materials,
Applications and Nanostructures,
Spain

Reviewed by:

Jeremy Teo,
New York University Abu Dhabi,
United Arab Emirates
Sônia Maria Malmonge,
Federal University of ABC, Brazil

*Correspondence:

Jeffrey R. Capadona
jrc35@case.edu
Evon S. Ereifej
eereifej@umich.edu

†These authors have contributed
equally to this work

Specialty section:

This article was submitted to
Biomaterials,
a section of the journal
Frontiers in Bioengineering and
Biotechnology

Received: 14 November 2019

Accepted: 14 April 2020

Published: 08 May 2020

Citation:

Mahajan S, Hermann JK,
Bedell HW, Sharkins JA, Chen L,
Chen K, Meade SM, Smith CS,
Rayyan J, Feng H, Kim Y,
Schiefer MA, Taylor DM,
Capadona JR and Ereifej ES (2020)
Toward Standardization of
Electrophysiology and Computational
Tissue Strain in Rodent Intracortical
Microelectrode Models.
Front. Bioeng. Biotechnol. 8:416.
doi: 10.3389/fbioe.2020.00416

Shreya Mahajan¹, John K. Hermann^{2,3†}, Hillary W. Bedell^{2,3†}, Jonah A. Sharkins^{4,5},
Lei Chen⁶, Keying Chen^{2,3}, Seth M. Meade^{2,3}, Cara S. Smith^{2,3}, Jacob Rayyan^{2,3},
He Feng^{2,3}, Youjoung Kim^{2,3}, Matthew A. Schiefer^{2,3}, Dawn M. Taylor^{2,3,7},
Jeffrey R. Capadona^{2,3*} and Evon S. Ereifej^{3,4,5,8*}

¹ Department of Electrical Engineering and Computer Science, University of Michigan, Ann Arbor, MI, United States,

² Department of Biomedical Engineering, Case Western Reserve University, Cleveland, OH, United States, ³ Advanced Platform Technology Center, Louis Stokes Cleveland Veterans Affairs Medical Center, Cleveland, OH, United States,

⁴ Veteran Affairs Ann Arbor Healthcare System, Ann Arbor, MI, United States, ⁵ Department of Biomedical Engineering, University of Michigan, Ann Arbor, MI, United States, ⁶ Department of Mechanical Engineering, University of Michigan, Ann Arbor, MI, United States, ⁷ Department of Neuroscience, The Cleveland Clinic, Cleveland, OH, United States, ⁸ Department of Neurology, University of Michigan, Ann Arbor, MI, United States, ⁹ Functional Electrical Stimulation Center, Louis Stokes Cleveland Veterans Affairs Medical Center, Cleveland, OH, United States

Progress has been made in the field of neural interfacing using both mouse and rat models, yet standardization of these models' interchangeability has yet to be established. The mouse model allows for transgenic, optogenetic, and advanced imaging modalities which can be used to examine the biological impact and failure mechanisms associated with the neural implant itself. The ability to directly compare electrophysiological data between mouse and rat models is crucial for the development and assessment of neural interfaces. The most obvious difference in the two rodent models is size, which raises concern for the role of device-induced tissue strain. Strain exerted on brain tissue by implanted microelectrode arrays is hypothesized to affect long-term recording performance. Therefore, understanding any potential differences in tissue strain caused by differences in the implant to tissue size ratio is crucial for validating the interchangeability of rat and mouse models. Hence, this study is aimed at investigating the electrophysiological variances and predictive device-induced tissue strain. Rat and mouse electrophysiological recordings were collected from implanted animals for eight weeks. A finite element model was utilized to assess the tissue strain from implanted intracortical microelectrodes, taking into account the differences in the depth within the cortex, implantation depth, and electrode geometry between the two models. The rat model demonstrated a larger percentage of channels recording single unit activity and number of units recorded per channel at acute but not chronic time points, relative to the mouse model. Additionally, the finite element models also revealed no predictive differences in tissue strain between the two rodent models. Collectively

our results show that these two models are comparable after taking into consideration some recommendations to maintain uniform conditions for future studies where direct comparisons of electrophysiological and tissue strain data between the two animal models will be required.

Keywords: rodent model, intracortical microelectrodes, electrophysiology, tissue strain, brain, finite element model

INTRODUCTION

Intracortical microelectrodes (IMEs) allow for direct interfacing with neuronal populations, thereby enabling the exploration of neuronal function, neurological diseases, and potential therapies (Wise and Angell, 1975; Schwartz, 2004; Kipke et al., 2008). Intracortical microelectrodes are able to record and transmit electrical impulses directly from neurons in the brain (Renshaw et al., 1940). Recorded electrical impulses can then be used in numerous applications, including being translated into control signals for prosthetic devices to restore function (Hochberg et al., 2006; Schwartz et al., 2006; Gilja et al., 2015). When used in brain–machine interfacing (BMI) applications, IMEs have enabled quadriplegic and amyotrophic lateral sclerosis (ALS) patients to control external neuroprosthetic devices as well as neuromuscular stimulation systems that restore movement to their own limbs (Gilja et al., 2015; Schroeder and Chestek, 2016; Ajiboye et al., 2017). Intracortical microelectrodes have also been an essential part of many basic neuroscience studies and have significantly advanced our understanding of natural brain function.

The usefulness of IMEs depends on the ability to reliably record the electrical signals from many individual neurons over time (Wise, 2005; Kozai et al., 2015a; Ajiboye et al., 2017). The ability of IMEs to detect isolatable action potentials from individual neurons is directly dependent on the distance between healthy neuronal cell bodies and the microelectrode recording site (Buzsáki, 2004). The inflammatory response to implanted electrodes is thought to limit the ability to record consistent and reliable signals over time and contribute to electrode failure (Biran et al., 2005; McConnell et al., 2009; Potter et al., 2012; Kozai et al., 2015b). The complex inflammatory response occurring after electrode implantation results in decreased recording quality within weeks, and a continued decline often leading to complete loss of detectable action potentials within a few years (Chestek et al., 2011; Jorfi et al., 2015; Kozai et al., 2015b).

The initial insertion of IME causes breaching of the blood–brain barrier (BBB), which leads to injury of the local brain parenchyma (Potter et al., 2013; Saxena et al., 2013). Damage to the BBB is believed to be chronically agitated as stiff implants move against the natural micromotions of the brain observed during respiration and activity-dependent vasculature changes (Gilletti and Muthuswamy, 2006; Harris et al., 2011; Nguyen et al., 2014; Zhang et al., 2014; Prodanov and Delbeke, 2016). The breached BBB allows for the infiltration of blood-borne cells and the initiation of an inflammatory response (Ravikumar et al., 2014b; Bedell et al., 2018a). Chronic implantation of the IME

results in a frustrated phagocytic event, causing a build-up of pro-inflammatory factors (He et al., 2007; Skousen et al., 2015). Accumulations of pro-inflammatory molecules causes oxidative damage to the surrounding cells, tissue, and the IME (Ereifej et al., 2018; Bennett et al., 2019). Within weeks, the inflammatory response results in a glial scar which creates a barrier believed to reduce the ability of the IME to consistently record signals from local neurons (McConnell et al., 2009; Ravikumar et al., 2014b; Kozai et al., 2015b; Nguyen et al., 2016).

The early failures of IMEs have sparked substantial research in understanding electrode failure by utilizing several animal models and novel techniques. Studies involving feline models have shown unreliable and inconsistent electrode performance, with variability in recordings for up to 2 months, due to the instability of the electrode–tissue interface (Rousche and Normann, 1998; Xindong et al., 1999, 2006). Utilization of primates in IME studies have shown the potential clinical applications of the electrodes, but unfortunately suffer from the same decline in recording performance (Chestek et al., 2011; Barrese et al., 2013, 2016). Recent work introducing a marmoset model also displayed similar signal degradation found in traditional animal models (Debnath et al., 2018). Rodent models yield similar electrode reliability results compared to the larger animal alternatives. However, the smaller sized animals offer a less sentinel species with lower costs and smaller housing requirements, enabling larger sample sizes for increased statistical power. Therefore, rodents continue to be the most commonly utilized animal model to investigate the performance and integration of IME.

In turn, rats have been employed for years to better understand the failure mechanism after IME implantation (Vetter et al., 2004; Zhong and Bellamkonda, 2007; McConnell et al., 2009; Winslow and Tresco, 2010; Potter et al., 2012; Prasad et al., 2014; Nolte et al., 2015; Bennett et al., 2018; Ereifej et al., 2018; Salatino et al., 2019). Moreover, recent work has shown the ability to use rats to investigate motor functions following implantation of neural probes in the motor cortex (Goss-Varley et al., 2017, 2018). It is thought that rats are utilized more frequently in experiments compared to mice, due to their stronger physiological similarities to humans (Shanks et al., 2009) and ease in surgical procedures due to larger size (Barre-Sinoussi and Montagutelli, 2015).

While rat models have proven useful, there has been a recent move toward the use of mice when studying the acute and chronic performance of developing IME technologies. For examples, transgenic knock out studies are commonly performed in mice over rats due to cost and the availability of “off-the-shelf” engineered animals. Transgenic animal models enable researchers to target and better understand specific genes that

may affect electrode performance (Kozai et al., 2014; Bedell et al., 2018a,b; Hermann et al., 2018a,b). Additionally, mouse models have shown promise with optogenetic studies, aiding the ability to correlate the electrophysiology a specific cell to the observed behaviors (Anikeeva et al., 2011; Pashaie et al., 2014; Park et al., 2017). Mice are also ideal candidates for 2-photon microscopy, due to the smaller size of their brain allowing for live imaging into deeper structures of the brain. For example, 2-photon microscopy with mice has been used in the field of neural engineering to investigate the live cellular response along the depth of the implanted IME (Kozai et al., 2012, 2016).

As can be seen from the aforementioned examples, there are advantages to using both rats and mice when studying IME performance and the evoked tissue response. In fact, our lab has used both interchangeably (Ereifej et al., 2017, 2018; Bedell et al., 2018a, 2019; Hermann et al., 2018a; Mahajan et al., 2019). The initial intent of this study was to perform an internal check of consistency to ensure that we were justified in using both rodent models. Here, we report on our “internal audit” as a way to help standardize the field and ease any similar concerns, while preventing the unnecessary duplication of animal research. It is critical to validate the scaling and translation of findings from the mouse model to inform the design of experiments using rat models, and vice versa. Of note, other fields of research such as, diabetes, orthopedic, gene sequencing, among others, have shown the importance of validating the ability to use different animal models and compare them to one another while relating to the clinical models (Working, 1988; Giannobile et al., 1994; Newman et al., 1995; Yan et al., 2011; Islam et al., 2013). Particularly, previous work from our lab attempting to account for the animal model interchangeability has shown negligible differences of histological outcomes for glial cell activation, neuronal density and BBB breaching between the two models at initial (2 weeks) and chronic (16 weeks) time points (Potter-Baker et al., 2014). However, we have yet to investigate whether there are differences observed in electrophysiological recordings between the rat and mouse model. It is also of great interest to evaluate any implications the implanted electrodes have on the mechanical strain exerted on the adjacent brain tissue. It is hypothesized that there may be a direct relationship between the size of the electrode relative to the brain tissue and the resultant strain on the brain tissue. Therefore, this study is the first to utilize finite element modeling to compare tissue strain caused by IMEs in both the rat and mouse model, as well as comparisons of the electrophysiological recordings made from the two models over 8 weeks under similar conditions.

MATERIALS AND METHODS

Intracortical Microelectrode Implantation Procedure

Similar silicon, single shank, 16 channel IMEs from NeuroNexus were utilized in both rodent models but with different inter-electrode-contact spacing to account for differences in cortical thickness. Specifically, the rat model used probe model # A1 × 16-3mm-100-177-Z16, with inter-contact spacing of 100 μm, while

the mice were implanted with probe model # A1 × 16-3mm-50-177-Z16, which had an inter-contact spacing of 50 μm. Prior to implantation, electrode impedance magnitudes were measured at 1 kHz in saline and verified to the manufacturer's values. Electrodes were then washed with a mixture of 95% ethanol and deionized water for 5 min and air dried. Implants were then sterilized using the standard ethylene oxide (EO) gas protocol: 54.4° F, 1 h sterile time and 12 h aerate (Ravikumar et al., 2014a).

The Institutional Animal Care and Use Committees (IACUC) at the Louis Stokes Cleveland Veterans Affairs Medical Center (LSCDVAMC) and Case Western Reserve University (CWRU) approved all animal procedures. All rat work was performed at LSCDVAMC by one surgeon, while mouse work was performed at CWRU by two other surgeons; all three surgeons have the same expert level competency for performing these surgeries. Six male Sprague Dawley rats (8–10 weeks old and weighing ~225 g) and 14 male/female C57/BL mice (8–10 weeks old and weighing ~20g) were utilized in this study. Implantation procedures were similar for both animal models with a few minor differences due to protocol requirements for other ongoing studies. Both animal models used isoflurane to anesthetize the animals to the surgical plane prior to surgery, (3.5% in 1.5 L/min O₂ for rats and 3% in 1.0 L/min O₂ for mice). Surgical procedures for mice were performed in a class II sterile hood using microisolator techniques, whereas the rat surgeries were done on an open surgical table using aseptic techniques. Animals were prepped for surgery by first shaving the implantation site, and then sterilizing the area with alternating wipes of betadine for mice and chlorhexidine gluconate (CHG) for rats, and isopropanol. Marcaine (0.2 mL of 0.25% Marcaine) was administered subcutaneously (SQ) around the surgical site as a topical anesthetic. For antibiotics and analgesic, Cefazolin (25 mg/kg in rats), Carprofen (5 mg/kg for rats), and Meloxicam (2 mg/kg in mice) were administered subcutaneously. Animals were then mounted on a stereotaxic frame and maintained at the surgical plane by inhalation of 0.5–2% isoflurane through a nosecone throughout the surgery.

In both animal models, an incision was made down the midline of the scalp and the skin was retracted to expose the skull. The skull was cleaned of the periosteum, dehydrated using hydrogen peroxide, and primed using Vetbond animal tissue adhesive. Three craniotomies were drilled, one each for the ground wire, reference wire and electrode. A 0.45 mm drill bit was used for all craniotomies, except for the electrode craniotomy in rats, which was 2 mm in diameter. Because the dura was too thick for the silicon electrodes to penetrate in the rat model, the dura was reflected prior to implanting the electrode in the rat. Due to the size difference between the rat and mouse skull, the coordinates for the craniotomies differed slightly. In rats, the ground wire was 1.5 mm lateral to midline and 1.5 mm posterior to bregma, the reference wire was 1.5 mm lateral to midline and 5.5 mm posterior to bregma, and the electrode craniotomy was on the contralateral side, 2 mm lateral to midline and 2 mm anterior to bregma (forelimb primary motor cortex). In mice, the ground wire was 1.5 mm lateral to midline and 1 mm rostral to the bregma and the reference wire was 1.5 mm lateral to midline and 1 mm caudal to the bregma, and the electrode

craniotomy was on the contralateral side, 1.5 mm lateral and 0.5 mm anterior or posterior to the bregma (motor/sensorimotor cortex). The ground and reference wires were manually inserted and secured to the skull (rats used Teets cold cure dental cement and mice used silicone elastomer and Stoelting dental cement). The electrodes were implanted using a Kopf micromanipulator. In rats, the implant insertion rate was 100 μm (the distance between channels) every 1–2 min up to an approximate depth of 2000 μm , which ensured that the length of the electrode containing the 16 contacts spanned across layers III–V of the cortex containing the majority of the detectable pyramidal cells. In mice, the electrodes were inserted in increments of 50 μm (the distance between channels) at a rate of 10 $\mu\text{m}/\text{s}$, with intervals of 10–30 s in between. The electrode was implanted to a depth of approximately 1000 μm , to ensure that the contact sites of the electrode were present in cortical layers III–V. The electrode craniotomies were then sealed with a silicone elastomer (Kwik-Sil, World Precision Instruments) and a dental acrylic (Teets in rats, Stoelting in mice) was used to secure the electrode connector and form a sturdy headcap. Post-operative care and monitoring was provided the week following surgery, with administration of analgesia and antibiotics for up to three days following surgery.

Electrophysiological Recordings

Awake and freely moving tethered electrophysiological recordings were collected from the animals after surgical recovery. Recordings were taken using the TDT RZ5D BioAmp Processor recording system for the rat study, and TDT RX5 Pentusa Processor for the mouse studies. Prior to recordings, animals were anesthetized using 3% isoflurane when connecting the headstage cable to minimize head movement that could lead to connector damage. Ten minute recordings from each rat were collected twice per week starting the day after surgery continuing for 8 weeks, whereas 3 min recordings were obtained from each mouse twice per week beginning 5 days post-surgery until 16 weeks post-implantation. For direct comparison to the rat model, only the same 8 week duration is presented here.

Signal Processing

The electrophysiological data were processed as previously published, by implementing a sampling rate of 24.4 kHz, a bandpass filter spanning 300 Hz to 3 kHz and a common average reference algorithm (Bedell et al., 2018a; Hermann et al., 2018b). In order to account for some inherent variance in the final implanted electrode depth between animals (e.g., due to differences in brain swelling during implantation), performance metrics were calculated using the most active electrode contacts presumed to span the layers with the large pyramidal neurons. In rats the 10 consecutive channels having the most spiking activity (defined by the highest sum of average units over the 8 week study) were utilized for the final rat data assessment. Due to the smaller cortical thickness in mice, metrics for the mice were calculated using the eight consecutive channels with the highest sum of average units over time.

To address artifacts attributed to motion, moisture shorting head stage contacts, and inconsistent connections between recording equipment and arrays in an objective manner,

blinded artifact removal techniques were applied as previously described in detail (Bedell et al., 2018a; Hermann et al., 2018b). Artifact removal techniques administered by reviewer without knowledge of type of subject or time point included removal of time segments, channels, or recording sessions. In both rats and mice, the removed days and channels were randomly distributed across channels, days and animals groups (rat data removed = 1.04% of recording days and 1.25% of individual channels; mouse data removed = 9.7% of recording days and 2.6% of individual channels).

Following artifact removal, spikes were detected with a threshold of 3.5 standard deviations from the mean voltage. Snippets of data spanning 12 samples pre-threshold crossing to 24 samples post-threshold crossing were clustered by the unsupervised sorting algorithm, Wave_clus (Quiroga et al., 2004; Bedell et al., 2018a; Hermann et al., 2018b). The number of single unit clusters identified by the sorting algorithm was logged for each channel of the microelectrode array. Information about the number of clusters detected and signal quality of each cluster was used to generate five metrics for quantitative comparison (as described in Bedell et al. (2018a), Hermann et al. (2018b)). The first three metrics were calculated from all “working” channels (i.e., channels having impedances and noise levels consistent with intact connections): (1) percentage of working channels detecting single units, (2) average number of units per working channel, and (3) background noise level averaged across all working channels where noise level was calculated as twice the standard deviation of the background activity after time windows containing spikes and artifacts were removed [robust methods from Quiroga et al. (2004)]. Two additional metrics were calculated from the subset of channels detecting isolatable single units: (4) peak-to-peak maximum amplitude of each unit’s mean waveform averaged across all units on a given channel and (5) signal-to-noise ratio (SNR) averaged across units where the “signal” is each unit’s mean peak-to-peak amplitude and noise is calculated as in (3).

Strain Model

To investigate the difference between rats and mice in the tissue strain caused by brain micromotion after electrode implantation, three-dimensional (3D) finite-element models simulating interfacial strains induced by brain micromotion from respiration and vasculature were developed. We utilized a model that consisted of two components: a silicon-based single probe shank (dimensions and insertion depths relative to the electrodes used in the rat and mouse surgeries, respectively) and surrounding brain tissue (dimensions relative to animal’s respective cortex size), as shown in **Figure 1**. The cross-sectional dimensions of the brain tissue surrounding the electrode are two magnitudes higher than the probe cross-sectional area, ensuring that the boundaries will have negligible impact on the results, and only the depth of the electrode in relation to the cortex will be a variable taken into consideration in this model. In this study, the cortex was assumed to be linearly elastic with isotropic material properties to induce the primary strains in the surrounding tissue after electrode implantation. **Table 1** summarizes the dimensions and material properties used for the two components in both

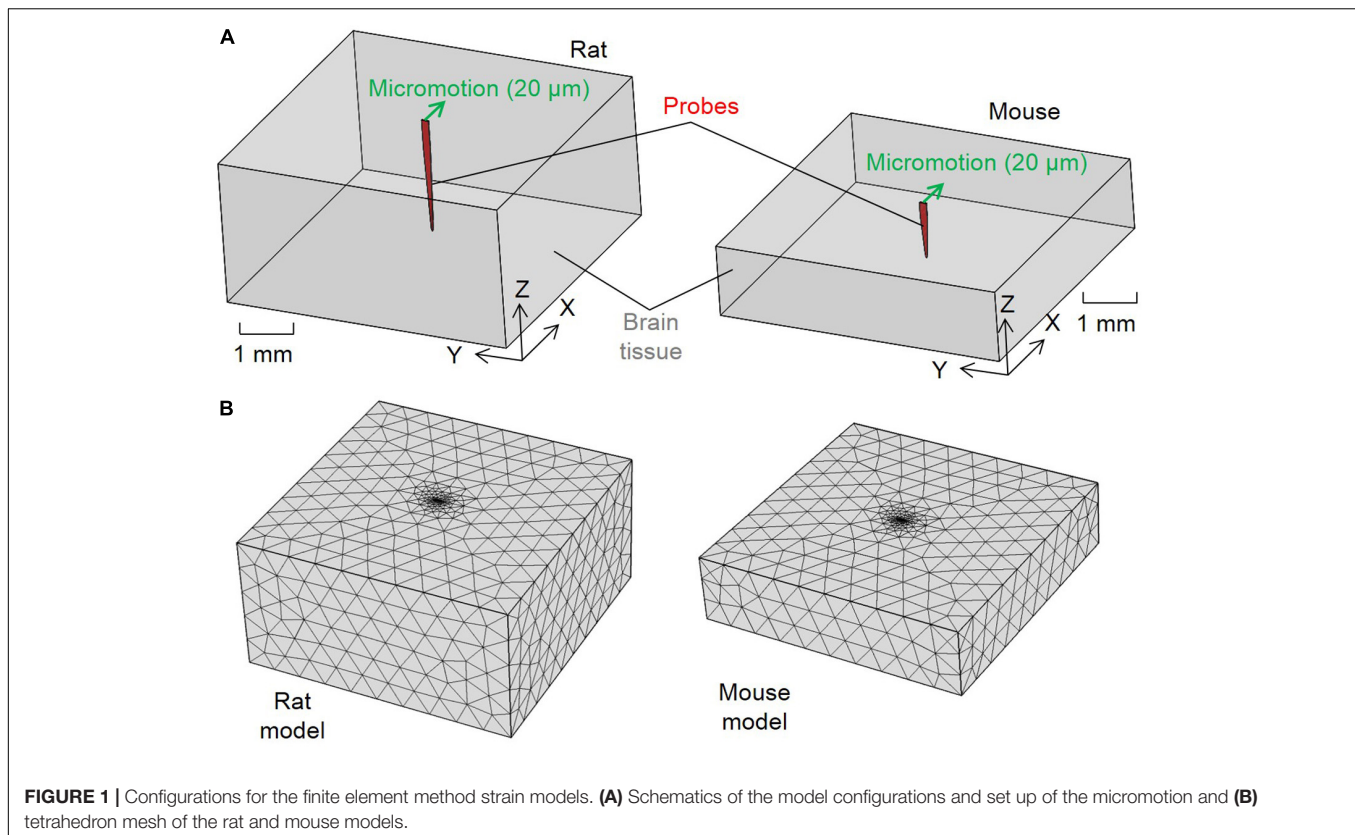


FIGURE 1 | Configurations for the finite element method strain models. **(A)** Schematics of the model configurations and set up of the micromotion and **(B)** tetrahedron mesh of the rat and mouse models.

models, as described previously (Subbaroyan et al., 2005; Nguyen et al., 2014). Recent work investigating the mechanical properties of various brain tissue specimens utilized in traumatic brain injury models, revealed no significant differences of viscoelastic properties between the rat and mouse cortical tissue (MacManus et al., 2017). Thus suggesting it is suitable to use the same Young's modulus and Poisson's ratio for the rat and mouse in our computational model.

The brain and electrode components were treated as one connected unit in both models by assuming tied contacts at the probe–brain interface. The bottom and side outer surfaces of the brain tissue were fixed in all directions as model boundary conditions. To simulate the relative tangential tethering, micromotion between the skull and brain tissue from an implant fixed to the skull, a 20 μm displacement along the positive X direction was applied to the top of the probe's shank. This simulated the displacement due to the relative micromotion between the skull and brain tissue, as marked by the green arrows in **Figure 1A**. Similar models investigating tissue strain after microelectrode implantation utilized 20 μm micromotion, which falls in the range of vascular (2–4 μm) and respiratory (10–30 μm) micromotion, as well as the calculated induced electrode displacement (20 μm) following rotational acceleration of an animal's head (Muthuswamy et al., 2003; Lee et al., 2005; Subbaroyan et al., 2005; Gilletti and Muthuswamy, 2006; Sridharan et al., 2013; Nguyen et al., 2014).

The two components were meshed into tetrahedron elements (**Figure 1B**). Brain tissue elements away from the interface for

both the rat and mouse models had mesh sizes of about 500 μm. A finer mesh was used to model the probe and area surrounding the interface elements with an average size of 83.27 μm. The meshing methodology generated in total 2,589 nodes and 13,495 elements for the rat model and 1,507 nodes and 7,347 elements for the mouse model. Strain distribution induced in the meshed models are as shown in **Figure 1B**. Strain distributions induced by the micromotion were solved using COMSOL Multiphysics software (COMSOL, Burlington, MA, United States). Strain distribution was described by von Mises strain, ϵ_e , which was calculated following the equation (Lee et al., 2005):

$$\epsilon_e = \frac{1}{1 + \nu} \left\{ \frac{1}{2} [(\epsilon_1 - \epsilon_2)^2 + (\epsilon_2 - \epsilon_3)^2 + (\epsilon_3 - \epsilon_1)^2] \right\}^{\frac{1}{2}} \quad (1)$$

where ν is the Poisson's ratio of the brain tissue and ϵ_1 , ϵ_2 , and ϵ_3 are first, second, and third principal strains correspondingly from output of the finite element method model as described in section "Strain Model". The von Mises strain fields obtained through Eq. (1) were then normalized by dividing all of the von Mises strain values by the maximum induced von Mises strain values across the entire models for both rat and mouse. The maximum induced von Mises strain value was found at the probe tip of the mouse model. The final von Mises strain values then ranged between zero and one allowing for impartial comparison between the two models.

TABLE 1 | Parameters used in the finite-element models to simulate micromotion and strain from implanted silicon probe shank in rat and mouse brain.

Components	Parameter	Rat model	Mouse model
Brain Tissue	Young's Modulus		6 KPa
	Poisson's ratio		0.43
	Dimension (X × Y × Z)	5000 μm × 5000 μm × 2500 μm	5000 μm × 5000 μm × 1250 μm
Silicon Probe Shank	Young's Modulus		200 GPa
	Poisson's ratio		0.27
	Dimension	Thickness = 15 μm, Max width = 123 μm narrowing down to 33 μm over a 1500 μm length and a 50 μm long tapering end	Thickness = 15 μm, Max width = 123 μm narrowing down to 33 μm over a 750 μm length and a 50 μm long tapering end
	Inter-channel length	100 μm	50 μm
	Insertion depth	2000 μm	1000 μm
	Prescribed displacement (due to micromotion)	20 μm	

Statistical Analysis

For statistical analysis of the five electrophysiology metrics, a general linear model in Minitab 16 (Minitab Inc., State College, PA, United States) was utilized to allow for comparisons between conditions (time and animal group) as fixed factors. Time was grouped in three ranges, total time (weeks 1–8), acute (weeks 1–2), and chronic (weeks 3–8) to represent the phases of the neuroinflammatory response at the neural interface (Reichert, 2007; Potter et al., 2012). To account for repeated measures, each individual rat or mouse was nested within its respective animal group. The terms of the model were the animal group and the different time intervals. Significance was defined as $p < 0.05$. Statistical analysis on the finite element strain models was performed by a Pearson correlation between the rat and mouse model.

RESULTS

Electrophysiological Recordings

Variability in Recordings

One of the main challenges to successful IME implementation is obtaining consistent recording quality. Inconsistent recording quality over time within the same animal, as well as between animals within the same group has been observed with previous studies utilizing one animal species (Rousche and Normann, 1998; Xindong et al., 1999, 2006; Chestek et al., 2011; Barrese et al., 2013, 2016; Michelson and Kozai, 2018). To our knowledge, a direct comparison of electrophysiological recording quality between two different animal species has not been previously reported. Here, our evaluation of the rat and mouse models revealed that both have variability within their own animal group, over time, and compared to one another (Figure 2).

Electrophysiological Results

Electrophysiological recordings from the rat model were compared to the mouse model over the entire course of time (weeks 1–8), as well as group based on the time course of

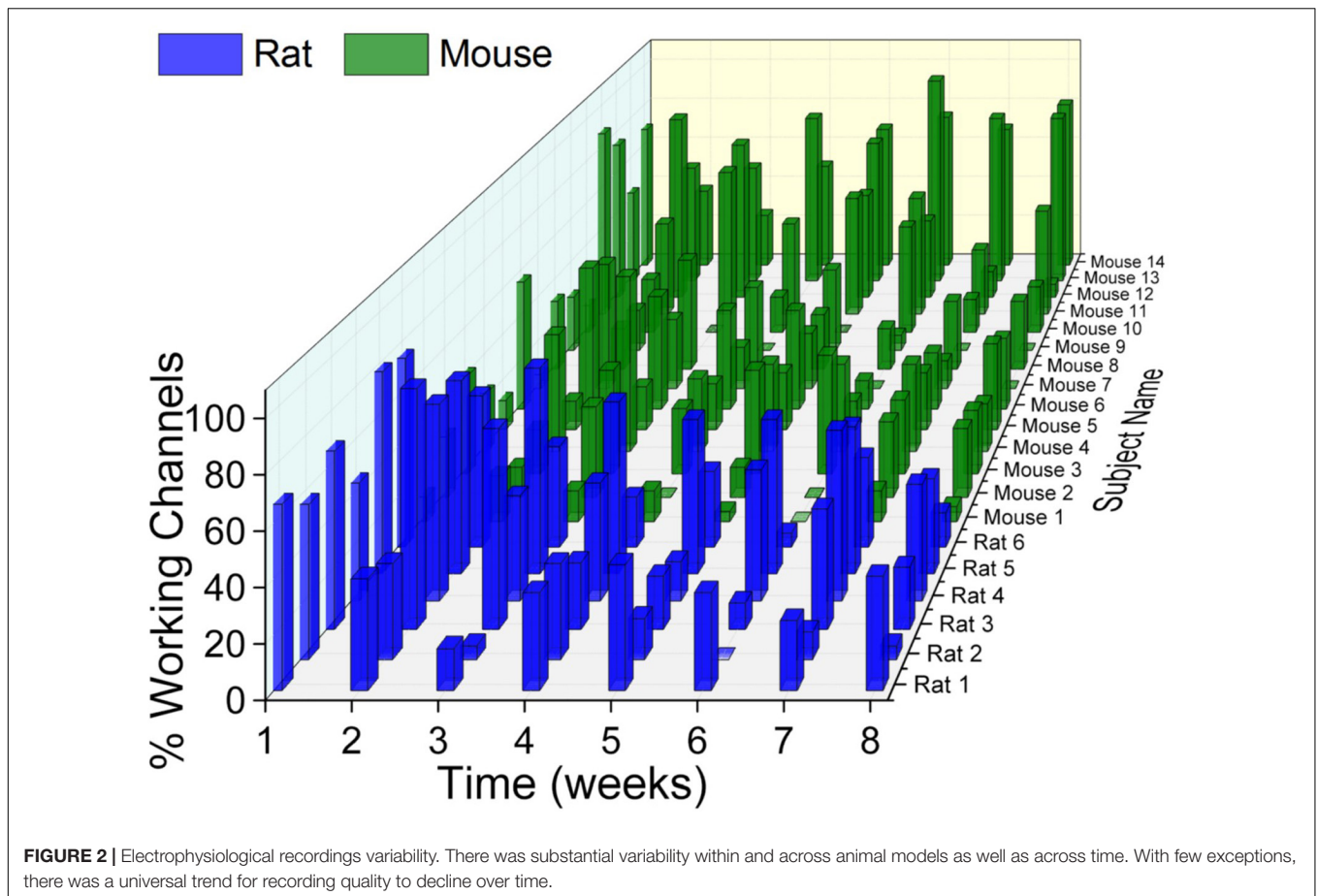
inflammatory events following device implantation: acute (weeks 1–2) and chronic (weeks 3–8) time points.

There was a significant difference (*indicates $p < 0.05$) in the percentage of channels recording single units and the single units recorded per channel between the rat and mouse models over the entire 8 weeks (Figures 3A,B). Further evaluation revealed there were significantly higher (#indicates $p < 0.05$) percentage of channels recording single units and single units recorded per channel in the rat model during the acute time point compared to the mouse model (Figures 3A,B). There were no significant differences of percentage of channels recording single units or single units recorded per channel between the two rodent models during the chronic time points (Figures 3A,B).

There was a significant difference (*indicates $p < 0.05$) of recorded noise between the rat and mouse models over the entire 8 weeks (Figure 3C). Yet, there were no significant differences in recorded noise between the two rodent models during the acute time points (Figure 3C). It was found that there was significantly more (#indicates $p < 0.05$) noise recorded in the mouse model compared to the rat model during the chronic time point (Figure 3C). There were no significant differences found between the recorded maximum amplitude (Figure 3D) or SNR (Figure 3E) between the rat and mouse recordings over the entire eight weeks or when compared at acute and chronic time intervals.

Finite Element Analysis of Tissue Strain

Normalized von Mises strain results are as shown in Figure 4. Simulated micromotion around the tethered probe resulted in elevated strains at the tissue surrounding both the top of the brain and tip of the probe (Figures 4A,B). Both animal models predicted to have similar strain profiles to each other around the tissue surrounding the top of the brain, and the mid-point and tip of the probe with a Pearson correlation coefficient of 0.97 (Figures 4C–E). It was found that the highest strain was at the tissue surrounding the top of the brain in both rat and mouse models (Figure 4C).



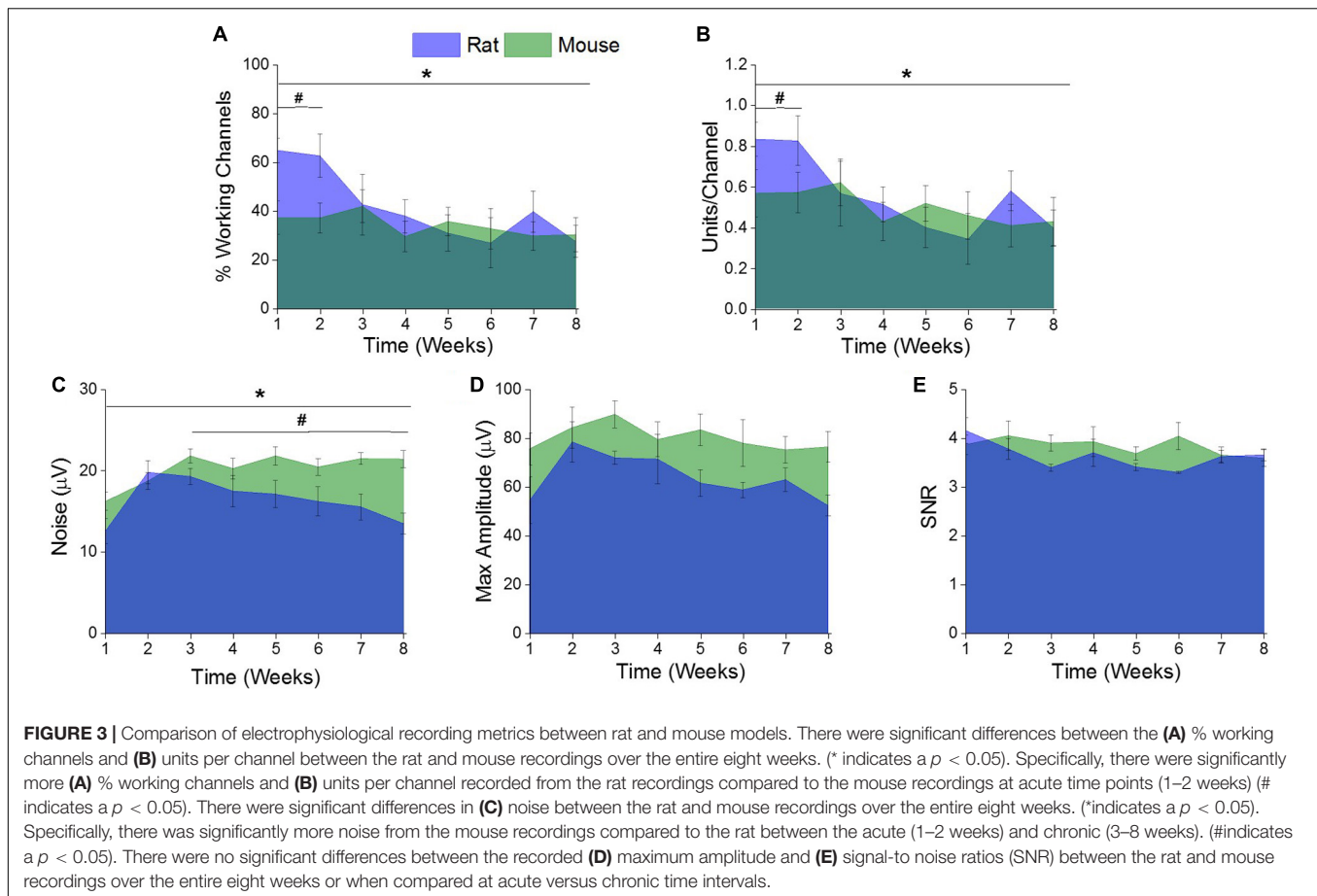
DISCUSSION

One of the main challenges of clinical implementation of IME technology is the instability and decline in recording signal (Biran et al., 2005; McConnell et al., 2009; Potter et al., 2012; Kozai et al., 2015b). The rat model is commonly utilized for understanding the decline of recording quality and longevity (Vetter et al., 2004; Nolte et al., 2015; Mahajan et al., 2019; Salatino et al., 2019), as well as for strategies to improve integration at the neural interface to expand electrophysiological outcomes (Jorfi et al., 2015; Kim et al., 2018; Wellman et al., 2018; Won et al., 2018). Recent progress has shown increased use of transgenic, optogenetic and two-photon techniques being employed more frequently in neural interface research (Anikeeva et al., 2011; Kozai et al., 2012, 2014, 2016; Pashaie et al., 2014; Luan et al., 2017; Park et al., 2017; Bedell et al., 2018a,b; Hermann et al., 2018a,b). As advances in neural interface research are made, it is becoming evident that the standardization of rat and mouse models is critical for translation of novel findings. Previous work has shown negligible inflammatory response differences using histological methods between these two animal models (Potter-Baker et al., 2014). However, as the neural interface field is expanding research strategies, it is necessary to further evaluate the differences between these two rodent models. Hence, we conducted a quantitative assessment of the electrophysiological

recordings and tissue strain from implanted IMEs in both rat and mouse models.

Electrophysiological recordings were taken twice per week for eight weeks, from awake, freely moving tethered rats and mice. In order to allow for direct comparison between the rat and mouse data, electrophysiological data was analyzed using the same metrics in both groups. Both rodent groups revealed a similar decline in electrode recording, with variability of recordings over time, within each rat and mouse group independently and between the two rodent groups comparatively. Although this observation is not optimal for IME translation, it is not surprising, as recording instability is known to be one of the main challenges with IME use. In fact, similar inconsistent recordings have been observed in other animal models, including cat and primate models (Rousche and Normann, 1998; Chestek et al., 2011; Barrese et al., 2013). It is noteworthy that both rodent models showed similar trends of signal decline and instability over the eight weeks. This indicates that the use of either rodent model will result in similar recording patterns, thus making the two models comparable.

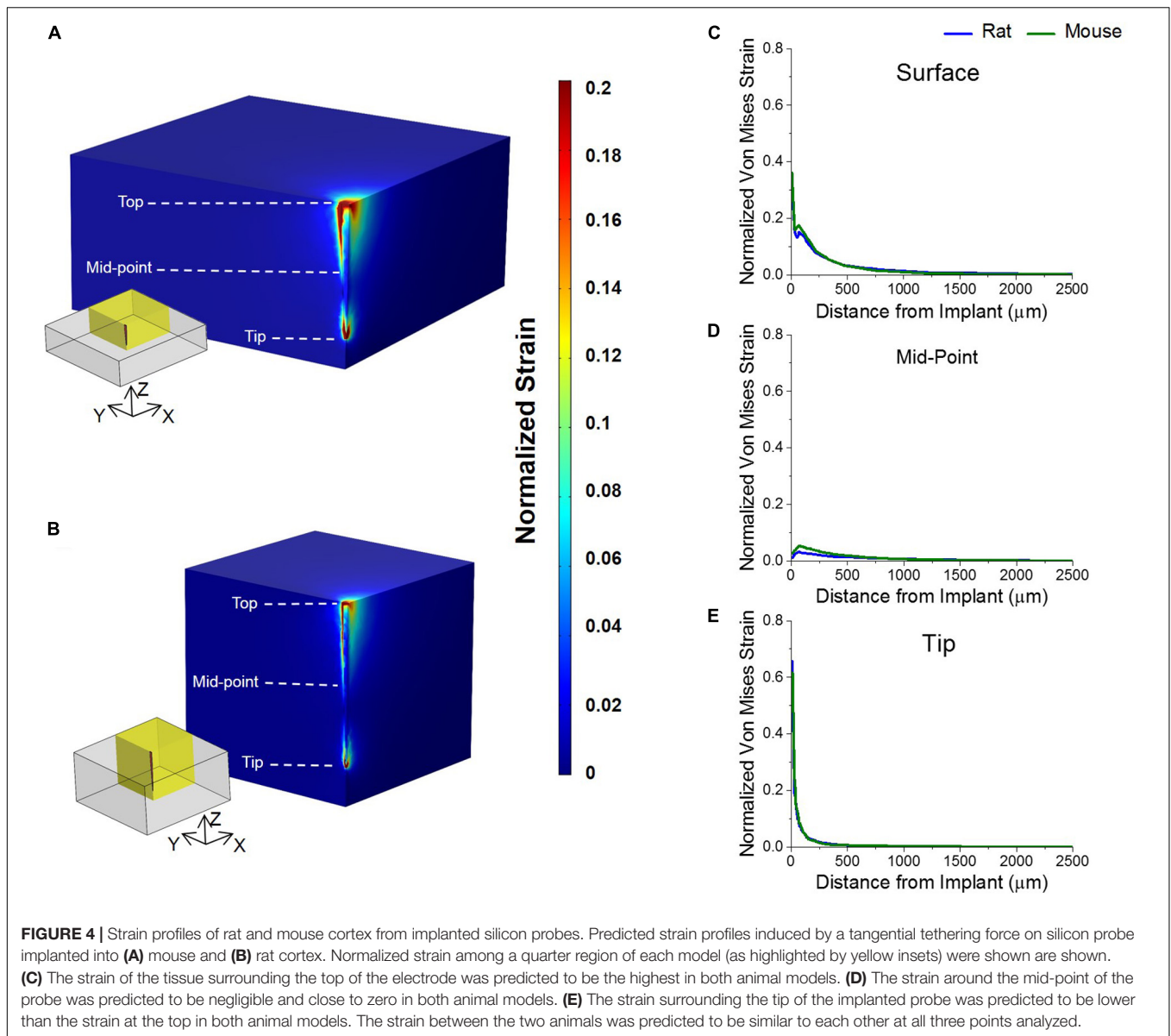
Differences in the percentage of channels recording single unit activity and the number of units recorded per channel between the rat and mouse model were noted within this study. Further analysis revealed these differences were only significant within the first two weeks of the study. In fact,



it was observed that the rat model had significantly higher percentage of channels recording single unit activity and the number of units recorded per channel in the first two weeks. However, the two animal models had overlapping trends for the remainder of the study. These observed differences can be explained by a few key differences between the animal models and surgical technique. First, the insertion rates between the two animal models varied slightly, with the rat insertion at 100 μm every 1–2 min and the mouse surgeries at a rate of 10 $\mu\text{m/s}$ every 10–30 s. It has recently been shown that slower insertion rates, 120 $\mu\text{m}/\text{min}$, results in improved recording quality, with the highest and most stable SNR, increased single unit yield, and the highest ratio of inhibitory interneurons at acute time points (1 and 45 min) (Fiáth et al., 2019). The insertion rate for the rat model was in line with the optimal insertion rates reported by Fiáth et al. (2019), indicating that the improved recordings observed during the first two weeks after implantation could be in part due to the slower insertion speed. It is thought that the slower insertion speed allows the brain tissue to recover from the necessary compression and stretching forces without breaching the BBB, which ultimately results in more neuronal survival around the implant (Edell et al., 1992; Bjornsson et al., 2006; Fiáth et al., 2019). Accordingly, the slower insertion speed used to implant into the rat may have actually allowed the brain tissue to partially recover during the insertion

time, thus resulting in improved recordings during the acute time point. There were no statistically significant differences of percentage of channels recording single unit activity and the number of units recorded per channel between the two rodent models beyond the acute time interval. This further suggests differences at the early time points were not due to inherent differences in the animal models themselves but due to temporary factors associated with implantation techniques. Additionally, it is common practice among some research groups to allow the rodents to recover from surgery for approximately one week prior to performing electrophysiological recordings, which our study did not incorporate, thus negating the acute recording differences observed herein (Nolta et al., 2015; White et al., 2016; Harris et al., 2017). Markedly, the duration of IME implantation for the majority of similar rodent studies is 12–16 weeks, emphasizing the importance of having comparable recordings between the rat and mouse models during the chronic time period (Kozai et al., 2014; Kozai et al., 2015a; Bedell et al., 2018a; Hermann et al., 2018b; Usoro et al., 2019). Furthermore, clinical trials utilizing implanted IMEs remain implanted on a timescale of years, underscoring the value of our chronic findings (Hochberg et al., 2006, 2012; Ajiboye et al., 2017).

The depth that the electrode was inserted varied between the two rodent models. Although the recording contacts on



the inserted electrode was proportional to the optimal cortical layers (layers III–V) of the respective rodent model, this variation may have resulted in the acute increase of percentage of channels recording single unit activity and the number of units recorded per channel in the rat model. In a previous study examining the inflammatory response to implanted electrodes between rat and mouse models, it was observed that there were significantly more neurons around the implanted probe in the rat cortex at two weeks compared to the mouse cortex (Potter-Baker et al., 2014). This observation was attributed to the difference in scale between the two animal models, specifically, the thickness of the cortical tissue, size of the cortical layers and the distribution of cells within that space (Defelipe, 2011; Potter-Baker et al., 2014). Furthermore, the variances of the single unit activity between the two animal models can also be attributed to the number of synaptic inputs per neuron in

each animal model (DeFelipe et al., 2002; Defelipe, 2011). As follows, this calculated synaptic activity per neuron in various animal models has revealed variances between animal models and cortical layers within the same animal model (DeFelipe et al., 2002; Defelipe, 2011). In fact, there are specific differences in the proportion, length, and density of putative excitatory and inhibitory synapses, which may not affect cortical layers the same, between the rat and mouse (Defelipe, 2011). Although the dissimilarities between the rat and mouse brain scale and synaptic activity could have been a source to the observed differences in electrophysiological recordings, further investigation into this hypothesis is required prior to concluding the observed electrophysiological differences between the two rodent models is due to inherent anatomy and physiology of the animals. The fact that there were no observed significant differences in the chronic recording metrics of percentage of channels recording

single unit activity, number of units recorded per channel, SNR and amplitude between the two rodent models would suggest the cyto-architecture differences between models may only have a limited effect on recording differences. The greater increase in recorded noise with the mouse model compared to the rat model may have been confounded by differences in environmental noise between the two models since the mice recordings were performed in a class II sterile hood and the rats were recorded on a non-enclosed surgical table. Hence, the overall electrophysiological results comparing the rat and mouse model show negligible differences between the two models and encourage future investigations to utilize either or both animal models.

In order to predict the micromotion induced strains surrounding the implanted probe, a finite element model simulating a 20 μm displacement to the top of the probe was utilized. The differences in electrode implantation depth, thickness of the cortex, and marginal variances in electrode geometry were all taken into consideration in the models. Interestingly, there were negligible differences between the predicted strain for the two rodent models. These results indicate that the strain induced onto the tissue from respiratory and vasculature micromotion is negligible between the rat and mouse. Both models displayed similar strain profiles with the highest being at the top of the brain (i.e., top of the probe), similar to our previous findings (Nguyen et al., 2014). Conversely, a variable that was not included in the model, but differed between the two rodent models is the reflection of the dura. During the rat surgeries, the dura is reflected to allow for ease of electrode insertion due to the stiffness of the dura. However, in the mouse, the dura is much thinner and removal is not necessary for electrode implantation. The influence reflection of the dura has on tissue strain, micromotion, and downstream inflammatory response is not fully understood, but likely has some effect initially before the dura regrows over time. In fact, Gilletti and Muthuswamy (2006) showed the presence of the dura exhibited a significantly lower respiratory displacement of rat brain tissue, compared to animals without a dura. However, the presence of the dura had no effect on the vasculature displacement (Gilletti and Muthuswamy, 2006). Our model did not take into account the different displacement values between the rat with a reflected dura and the mouse with an intact dura. Our model used total displacement, combining the effects of both vasculature and respiration, since the vasculature displacement has not been shown to be influenced by dura reflection; we kept the displacement value constant for both models. In future work, experimental measurements of displacement from both rat and mouse under conditions of reflected or intact dura will be conducted and the experimental data will be used as model inputs to define the brain micromotion. Future finite element models can incorporate multi-physics models, in which the effect of tissue strain from physiological micromotion and/or material stiffness can be correlated to the electrophysiological recordings. In fact, Lempka et al. (2011) utilized multi-physics computational modeling to investigate potential factors, such as electrode geometry and noise sources, to identify their effect

on recording quality. The effects on electrophysiology from pathophysiology of the brain, such as the formed glial scar, can also be assessed through multi-physics models. For instance, computational modeling from Malaga et al. (2015) discovered that the glial scar did not contribute to the reduction of signal amplitude, instead it was suggested that the displacement of neurons from the electrode was the main contributor to the size of the amplitude (Malaga et al., 2015). The work by Malaga et al. (2015) in combination with the total findings from Potter-Baker et al. (2014) demonstrating significantly more neurons around the implanted probe in the rat cortex at two weeks and the current findings herein signifying improved recording quality from the rat during the first two weeks, alludes that the improved recordings in the rat model are possibly due to less neuronal displacement after electrode implantation. Future multiple physics computational modeling, as well as experimental approaches, can further assess the acute neuronal displacement and coinciding electrophysiological recordings between animal models, while also taking into consideration the effects from reflection of the dura, tissue strain, glial scar, among many other variables.

CONCLUSION

Collectively the electrophysiological and predictive tissue strain data reveal there are negligible differences between the rat and mouse models. The reported increase of percentage of channels recording single unit activity and the number of units recorded per channel between the rat and mouse model could be attributed to the differences in electrode insertion rate. However, this variance observed may also be due to inherent differences in animal scale and physiology, but this requires further investigation. Finally, the finite element model revealed negligible differences between the two rodent models tissue strain from implanted electrodes. Although, the reflection of the dura in the rat model was not directly compared to the intact dura in the mouse model, dural regrowth after implantation should make the two models representative of strain at chronic time points. The finite element model presented herein, although preliminary, can set the foundation for future multiple physics components to be incorporated into.

DATA AVAILABILITY STATEMENT

The datasets generated for this study are available on request to the corresponding author.

ETHICS STATEMENT

The animal study was reviewed and approved by the Institutional Animal Care and Use Committee (IACUC) at the Louis Stokes Cleveland Veterans Affairs Medical Center (LSCDVAMC) and Case Western Reserve University (CWRU).

AUTHOR CONTRIBUTIONS

EE and JC contributed substantially to the conception and design of the work, analysis, and interpretation of data for the work, drafting the manuscript for important intellectual content, approved the final version to be published and agreed to be accountable for all aspects of the work. JH and HB contributed to the set-up, performance and analysis of the mouse electrophysiology data, as well as contributed to the conception, design and interpretation of the work. JS and SM each drafted sections of the manuscript. SM, LC, JH, and MS contributed to the design, implantation, and interpretation of the finite element strain models. EE, CS, SMM, JR, KC, HF, YK, and DT helped with the set-up, acquisition and analysis of the rat electrophysiology data. All authors approved the final version to be published and agreed to be accountable for all aspects of the work.

FUNDING

This study was supported in part by Career Development Award – 1 #RX001664-01A1 (Ereifej) and Career Development Award – 2 #RX002628-01A1 (Ereifej), Merit Review Awards GRANT11422140 and Grant12418820 (Capadona) and Research Career Scientist Award #

GRANT12635707 (Capadona) from the United States (US) Department of Veterans Affairs Rehabilitation Research and Development Service. Additionally, this work was also supported in part by the National Institute of Health, National Institute of Neurological Disorders and Stroke 1R01NS082404-01A1, GRANT11144956, GRANT11345179, and GRANT12635723 (Capadona), the NIH Neuroengineering Training Grant # 5T-32EB004314-16 (Kirsch). The contents do not represent the views of the U.S. Department of Veterans Affairs, the National Institutes of Health, or the United States Government.

ACKNOWLEDGMENTS

JH, HB, JS, KC, SM, CS, JR, HF, and YK were all students during the time of this study. In addition to their academic standing, each of them maintained a Without Compensation (WOC) appointment at their respective VA facilities in order to facilitate their efforts toward collaborative efforts with Department of Veterans Affairs projects, or to use resources at a VA facility. Additionally, MS, DT, and EE all maintain (partial) employment at the Department of Veterans Affairs as Biomedical Engineers, when JC maintains a part-time VA appointment as a Research Career Scientist.

REFERENCES

- Ajiboye, A. B., Bolu Ajiboye, A., Willett, F. R., Young, D. R., Memberg, W. D., Murphy, B. A., et al. (2017). Restoration of reaching and grasping movements through brain-controlled muscle stimulation in a person with tetraplegia: a proof-of-concept demonstration. *Lancet* 389, 1821–1830. doi: 10.1016/S0140-6736(17)30601-3
- Anikeeva, P., Andalman, A. S., Witten, I., Warden, M., Goshen, I., Grosenick, L., et al. (2011). Optrode: a multichannel readout for optogenetic control in freely moving mice. *Nat. Neurosci.* 15, 163–170. doi: 10.1038/nn.2992
- Barrese, J. C., Aceros, J., and Donoghue, J. P. (2016). Scanning electron microscopy of chronically implanted intracortical microelectrode arrays in non-human primates. *J. Neural Eng.* 13:026003. doi: 10.1088/1741-2560/13/2/026003
- Barrese, J. C., Rao, N., Paroo, K., Triebwasser, C., Vargas-Irwin, C., Franquemont, L., et al. (2013). Failure mode analysis of silicon-based intracortical microelectrode arrays in non-human primates. *J. Neural Eng.* 10:066014. doi: 10.1088/1741-2560/10/6/066014
- Barre-Sinoussi, F., and Montagutelli, X. (2015). Animal models are essential to biological research: issues and perspectives. *Future Sci.* 1:Fso63. doi: 10.4155/fso.15.63
- Bedell, H. W., Hermann, J. K., Ravikumar, M., Lin, S., Rein, A., Li, X., et al. (2018a). Targeting CD14 on blood derived cells improves intracortical microelectrode performance. *Biomaterials* 163, 163–173. doi: 10.1016/j.biomaterials.2018.02.014
- Bedell, H. W., Song, S., Li, X., Molinich, E., Lin, S., Stiller, A., et al. (2018b). Understanding the effects of both CD14-mediated innate immunity and device/tissue mechanical mismatch in the neuroinflammatory response to intracortical microelectrodes. *Front. Neurosci.* 12:772. doi: 10.3389/fnins.2018.00772
- Bedell, H. W., Schaub, N., Capadona, J. R., and Ereifej, E. S. (2019). Differential expression of genes involved in the acute innate immune response to intracortical microelectrodes. *Acta Biomater.* 102, 205–219. doi: 10.1016/j.actbio.2019.11.017
- Bennett, C., Mohammed, F., Álvarez-Ciara, A., Nguyen, M. A., Dietrich, W. D., Rajguru, S. M., et al. (2019). Neuroinflammation, oxidative stress, and blood-brain barrier (BBB) disruption in acute Utah electrode array implants and the effect of deferoxamine as an iron chelator on acute foreign body response. *Biomaterials* 188, 144–159. doi: 10.1016/j.biomaterials.2018.09.040
- Bennett, C., Samikkannu, M., Mohammed, F., Dietrich, W. D., Rajguru, S. M., and Prasad, A. (2018). Blood brain barrier (BBB)-disruption in intracortical silicon microelectrode implants. *Biomaterials* 164, 1–10. doi: 10.1016/j.biomaterials.2018.02.036
- Biran, R., Martin, D. C., and Tresco, P. A. (2005). Neuronal cell loss accompanies the brain tissue response to chronically implanted silicon microelectrode arrays. *Exp. Neurol.* 195, 115–126. doi: 10.1016/j.expneurol.2005.04.020
- Bjornsson, C., Oh, S. J., Al-Kofahi, Y., Lim, Y., Smith, K., Turner, J., et al. (2006). Effects of insertion conditions on tissue strain and vascular damage during neuroprosthetic device insertion. *J. Neural Eng.* 3:196. doi: 10.1088/1741-2560/3/3/002
- Buzsáki, G. (2004). Large-scale recording of neuronal ensembles. *Nat. Neurosci.* 7:446.
- Chestek, C. A., Gilja, V., Nuyujukian, P., Foster, J. D., Fan, J. M., Kaufman, M. T., et al. (2011). Long-term stability of neural prosthetic control signals from silicon cortical arrays in rhesus macaque motor cortex. *J. Neural Eng.* 8:045005. doi: 10.1088/1741-2560/8/4/045005
- Debnath, S., Prins, N. W., Pohlmeier, E., Mylavarapu, R., Geng, S., Sanchez, J. C., et al. (2018). Long-term stability of neural signals from microwire arrays implanted in common marmoset motor cortex and striatum. *Biomed. Phys. Eng. Exp.* 4:055025. doi: 10.1088/2057-1976/aada67
- Del Felipe, J. (2011). The evolution of the brain, the human nature of cortical circuits, and intellectual creativity. *Front. Neuroanat.* 5:29. doi: 10.3389/fnana.2011.00029
- DeFelipe, J., Alonso-Nanclares, L., and Arellano, J. I. (2002). Microstructure of the neocortex: comparative aspects. *J. Neurocytol.* 31, 299–316. doi: 10.1023/a:1024130211265
- Edell, D. J., Toi, V., McNeil, V. M., and Clark, L. (1992). Factors influencing the biocompatibility of insertable silicon microshafts in cerebral cortex. *IEEE Trans. Biomed. Eng.* 39, 635–643. doi: 10.1109/10.141202
- Ereifej, E. S., Rial, G. M., Hermann, J. K., Smith, C. S., Meade, S. M., Rayyan, J. M., et al. (2018). Implantation of neural probes in the brain elicits oxidative stress. *Front. Bioeng. Biotechnol.* 6:9. doi: 10.3389/fbioe.2018.00009

- Ereifej, E. S., Smith, C. S., Meade, S. M., Chen, K., Feng, H., and Capadona, J. R. (2017). The neuroinflammatory response to nanopatterning parallel grooves into the surface structure of intracortical microelectrodes. *Adv. Funct. Mater.* 28:1704420.
- Fiáth, R., Márton, A. L., Mátyás, F., Pinke, D., Márton, G., Tóth, K., et al. (2019). Slow insertion of silicon probes improves the quality of acute neuronal recordings. *Sci. Rep.* 9:111. doi: 10.1038/s41598-018-36816-z
- Giannobile, W. V., Finkelman, R. D., and Lynch, S. E. (1994). Comparison of canine and non-human primate animal models for periodontal regenerative therapy: results following a single administration of PDGF/IGF-I. *J. Periodontol.* 65, 1158–1168. doi: 10.1902/jop.1994.65.12.1158
- Gilja, V., Pandarinath, C., Blabe, C. H., Nuyujukian, P., Simeral, J. D., Sarma, A. A., et al. (2015). Clinical translation of a high-performance neural prosthesis. *Nat. Med.* 21:1142. doi: 10.1038/nm.3953
- Gilletti, A., and Muthuswamy, J. (2006). Brain micromotion around implants in the rodent somatosensory cortex. *J. Neural Eng.* 3 189–195. doi: 10.1088/1741-2560/3/3/001
- Goss-Varley, M., Dona, K. R., McMahon, J. A., Shoffstall, A. J., Ereifej, E. S., Lindner, S. C., et al. (2017). Microelectrode implantation in motor cortex causes fine motor deficit: implications on potential considerations to brain computer interfacing and human augmentation. *Sci. Rep.* 7:15254. doi: 10.1038/s41598-017-15623-y
- Goss-Varley, M., Shoffstall, A. J., Dona, K. R., McMahon, J. A., Lindner, S. C., Ereifej, E. S., et al. (2018). Rodent behavioral testing to assess functional deficits caused by microelectrode implantation in the rat motor cortex. *J. Vis. Exp.* 138:57829. doi: 10.3791/57829
- Harris, A. Z., Golder, D., and Likhtik, E. (2017). Multisite electrophysiology recordings in mice to study cross-regional communication during anxiety. *Curr. Protoc. Neurosci.* 80, 8.40.1–48.40.21. doi: 10.1002/cpns.32
- Harris, J. P., Capadona, J. R., Miller, R. H., Healy, B. C., Shanmuganathan, K., Rowan, S. J., et al. (2011). Mechanically adaptive intracortical implants improve the proximity of neuronal cell bodies. *J. Neural Eng.* 8:066011. doi: 10.1088/1741-2560/8/6/066011
- He, W., McConnell, G. C., Schneider, T. M., and Bellamkonda, R. V. (2007). A novel anti-inflammatory surface for neural electrodes. *Adv. Mater.* 19, 3529–3533.
- Hermann, J. K., Lin, S., Soffer, A., Wong, C., Srivastava, V., Chang, J., et al. (2018a). The role of toll-like receptor 2 and 4 innate immunity pathways in intracortical microelectrode-induced neuroinflammation. *Front. Bioeng. Biotechnol.* 6:113. doi: 10.3389/fbioe.2018.00113
- Hermann, J. K., Ravikumar, M., Shoffstall, A. J., Ereifej, E. S., Kovach, K. M., Chang, J., et al. (2018b). Inhibition of the cluster of differentiation 14 innate immunity pathway with IAXO-101 improves chronic microelectrode performance. *J. Neural Eng.* 15:025002. doi: 10.1088/1741-2560/15/2/025002
- Hochberg, L. R., Bacher, D., Jarosiewicz, B., Masse, N. Y., Simeral, J. D., Vogel, J., et al. (2012). Reach and grasp by people with tetraplegia using a neurally controlled robotic arm. *Nature* 485, 372–375. doi: 10.1038/nature11076
- Hochberg, L. R., Serruya, M. D., Friehs, G. M., Mukand, J. A., Saleh, M., Caplan, A. H., et al. (2006). Neuronal ensemble control of prosthetic devices by a human with tetraplegia. *Nature* 442, 164–171. doi: 10.1038/nature04970
- Islam, M. S., Koya, D., and Portha, B. (2013). Animal models of diabetes and its associated complications. *J. Diabetes Res.* 2013:593204. doi: 10.1155/2013/593204
- Jorfi, M., Skousen, J. L., Weder, C., and Capadona, J. R. (2015). Progress towards biocompatible intracortical microelectrodes for neural interfacing applications. *J. Neural Eng.* 12:011001. doi: 10.1088/1741-2560/12/1/011001
- Kim, Y., Meade, S. M., Chen, K., Feng, H., Rayyan, J., Hess-Dunning, A., et al. (2018). Nano-architectural approaches for improved intracortical interface technologies. *Front. Neurosci.* 12:456. doi: 10.3389/fnins.2018.00456
- Kipke, D. R., Shain, W., Buzsáki, G., Fetz, E., Henderson, J. M., Hetke, J. F., et al. (2008). Advanced neurotechnologies for chronic neural interfaces: new horizons and clinical opportunities. *J. Neurosci.* 28, 11830–11838. doi: 10.1523/JNEUROSCI.3879-08.2008
- Kozai, T. D., Du, Z., Gugel, Z. V., Smith, M. A., Chase, S. M., Bodily, L. M., et al. (2015a). Comprehensive chronic laminar single-unit, multi-unit, and local field potential recording performance with planar single shank electrode arrays. *J. Neurosci. Methods* 242, 15–40. doi: 10.1016/j.jneumeth.2014.12.010
- Kozai, T. D. Y., Jaquins-Gerstl, A. S., Vazquez, A. L., Michael, A. C., and Cui, X. T. (2015b). Brain tissue responses to neural implants impact signal sensitivity and intervention strategies. *ACS Chem. Neurosci.* 6, 48–67. doi: 10.1021/cn500256e
- Kozai, T. D., Eles, J. R., Vazquez, A. L., and Cui, X. T. (2016). Two-photon imaging of chronically implanted neural electrodes: sealing methods and new insights. *J. Neurosci. Methods* 258, 46–55. doi: 10.1016/j.jneumeth.2015.10.007
- Kozai, T. D., Li, X., Bodily, L. M., Caparosa, E. M., Zenonos, G. A., Carlisle, D. L., et al. (2014). Effects of caspase-1 knockout on chronic neural recording quality and longevity: insight into cellular and molecular mechanisms of the reactive tissue response. *Biomaterials* 35, 9620–9634. doi: 10.1016/j.biomaterials.2014.08.006
- Kozai, T. D., Vazquez, A. L., Weaver, C. L., Kim, S. G., and Cui, X. T. (2012). In vivo two-photon microscopy reveals immediate microglial reaction to implantation of microelectrode through extension of processes. *J. Neural Eng.* 9:066001. doi: 10.1088/1741-2560/9/6/066001
- Lee, H., Bellamkonda, R. V., Sun, W., and Levenston, M. E. (2005). Biomechanical analysis of silicon microelectrode-induced strain in the brain. *J. Neural Eng.* 2, 81–89. doi: 10.1088/1741-2560/2/4/003
- Lempka, S. F., Johnson, M. D., Moffitt, M. A., Otto, K. J., Kipke, D. R., and McIntyre, C. C. (2011). Theoretical analysis of intracortical microelectrode recordings. *J. Neural Eng.* 8:045006. doi: 10.1088/1741-2560/8/4/045006
- Luan, L., Wei, X., Zhao, Z., Siegel, J. J., Potnis, O., Tuppen, C. A., et al. (2017). Ultraflexible nanoelectronic probes form reliable, glial scar-free neural integration. *Sci. Adv.* 3:e1601966. doi: 10.1126/sciadv.1601966
- MacManus, D. B., Pierrat, B., Murphy, J. G., and Gilchrist, M. D. (2017). Region and species dependent mechanical properties of adolescent and young adult brain tissue. *Sci. Rep.* 7, 1–12. doi: 10.1038/s41598-018-28932-7
- Mahajan, S., Sharkins, J. A., Hunter, A. H., Avishai, A., and Ereifej, E. S. (2019). Focused ion beam lithography to etch nano-architectures into microelectrodes. *J. Vis. Exp.* 155:e60004. doi: 10.3791/60004
- Malaga, K. A., Schroeder, K. E., Patel, P. R., Irwin, Z. T., Thompson, D. E., Bentley, J. N., et al. (2015). Data-driven model comparing the effects of glial scarring and interface interactions on chronic neural recordings in non-human primates. *J. Neural Eng.* 13:016010. doi: 10.1088/1741-2560/13/1/016010
- McConnell, G. C., Rees, H. D., Levey, A. I., Gutekunst, C.-A., Gross, R. E., and Bellamkonda, R. V. (2009). Implanted neural electrodes cause chronic, local inflammation that is correlated with local neurodegeneration. *J. Neural Eng.* 6:056003. doi: 10.1088/1741-2560/6/5/056003
- Michelson, N. J., and Kozai, T. D. (2018). Isoflurane and ketamine differentially influence spontaneous and evoked laminar electrophysiology in mouse V1. *J. Neurophysiol.* 120, 2232–2245. doi: 10.1152/jn.00299.2018
- Muthuswamy, J., Gilletti, A., Jain, T., and Okandan, M. (2003). “Microactuated neural probes to compensate for brain micromotion,” in *Proceedings of the 25th Annual International Conference of the IEEE Engineering in Medicine and Biology Society (IEEE Cat. No. 03CH37439)*, (Cancun: IEEE), 1941–1943.
- Newman, E., Turner, A., and Wark, J. (1995). The potential of sheep for the study of osteopenia: current status and comparison with other animal models. *Bone* 16, S277–S284. doi: 10.1016/8756-3282(95)00026-a
- Nguyen, J. K., Jorfi, M., Buchanan, K. L., Park, D. J., Foster, E. J., Tyler, D. J., et al. (2016). Influence of resveratrol release on the tissue response to mechanically adaptive cortical implants. *Acta Biomater.* 29, 81–93. doi: 10.1016/j.actbio.2015.11.001
- Nguyen, J. K., Park, D. J., Skousen, J. L., Hess-Dunning, A., Tyler, D. J., Rowan, S. J., et al. (2014). Mechanically-compliant intracortical implants reduce the neuroinflammatory response. *J. Neural Eng.* 11:056014. doi: 10.1088/1741-2560/11/5/056014
- Nolta, N. F., Christensen, M. B., Crane, P. D., Skousen, J. L., and Tresco, P. A. (2015). BBB leakage, astrogliosis, and tissue loss correlate with silicon microelectrode array recording performance. *Biomaterials* 53, 753–762. doi: 10.1016/j.biomaterials.2015.02.081
- Park, S., Guo, Y., Jia, X., Choe, H. K., Grena, B., Kang, J., et al. (2017). One-step optogenetics with multifunctional flexible polymer fibers. *Nat. Neurosci.* 20, 612–619. doi: 10.1038/nn.4510
- Pashaie, R., Anikeeva, P., Lee, J. H., Prakash, R., Yizhar, O., Prigge, M., et al. (2014). Optogenetic brain interfaces. *IEEE Rev. Biomed. Eng.* 7, 3–30. doi: 10.1109/RBME.2013.2294796
- Potter, K. A., Buck, A. C., Self, W. K., Callanan, M. E., Sunil, S., and Capadona, J. R. (2013). The effect of resveratrol on neurodegeneration and blood brain barrier

- stability surrounding intracortical microelectrodes. *Biomaterials* 34, 7001–7015. doi: 10.1016/j.biomaterials.2013.05.035
- Potter, K. A., Buck, A. C., Self, W. K., and Capadona, J. R. (2012). Stab injury and device implantation within the brain results in inversely multiphasic neuroinflammatory and neurodegenerative responses. *J. Neural Eng.* 9:046020. doi: 10.1088/1741-2560/9/4/046020
- Potter-Baker, K. A., Ravikumar, M., Burke, A. A., Meador, W. D., Householder, K. T., Buck, A. C., et al. (2014). A comparison of neuroinflammation to implanted microelectrodes in rat and mouse models. *Biomaterials* 35, 5637–5646. doi: 10.1016/j.biomaterials.2014.03.076
- Prasad, A., Xue, Q.-S., Dieme, R., Sankar, V., Mayrand, R. C., Nishida, T., et al. (2014). Abiotic-biotic characterization of Pt/Ir microelectrode arrays in chronic implants. *Front. Neuroeng.* 7:2. doi: 10.3389/fneng.2014.00002
- Prodanov, D., and Delbeke, J. (2016). Mechanical and biological interactions of implants with the brain and their impact on implant design. *Front. Neurosci.* 10:11. doi: 10.3389/fnins.2016.00011
- Quiroga, R. Q., Nadasdy, Z., and Ben-Shaul, Y. (2004). Unsupervised spike detection and sorting with wavelets and superparamagnetic clustering. *Neural Comput.* 16, 1661–1687. doi: 10.1162/089976604774201631
- Ravikumar, M., Hageman, D. J., Tomaszewski, W. H., Chandra, G. M., Skousen, J. L., and Capadona, J. R. (2014a). The effect of residual endotoxin contamination on the neuroinflammatory response to sterilized intracortical microelectrodes. *J. Mater. Chem. B* 2, 2517–2529.
- Ravikumar, M., Sunil, S., Black, J., Barkauskas, D. S., Haung, A. Y., Miller, R. H., et al. (2014b). The roles of blood-derived macrophages and resident microglia in the neuroinflammatory response to implanted intracortical microelectrodes. *Biomaterials* 35, 8049–8064. doi: 10.1016/j.biomaterials.2014.05.084
- Reichert, W. M. (2007). *Indwelling Neural Implants: Strategies for Contending With the in vivo Environment*. Boca Raton, FL: CRC Press.
- Renshaw, B., Forbes, A., and Morison, B. R. (1940). Activity of isocortex and hippocampus: electrical studies with micro-electrodes. *J. Neurophysiol.* 3, 74–105.
- Rousche, P. J., and Normann, R. A. (1998). Chronic recording capability of the Utah intracortical electrode array in cat sensory cortex. *J. Neurosci. Methods* 82, 1–15.
- Salatino, J. W., Kale, A. P., and Purcell, E. K. (2019). Alterations in ion channel expression surrounding implanted microelectrode arrays in the brain. *bioRxiv* [Preprint] doi: 10.1101/518811
- Saxena, T., Karumbaiah, L., Gaupp, E. A., Patkar, R., Patil, K., Betancur, M., et al. (2013). The impact of chronic blood-brain barrier breach on intracortical electrode function. *Biomaterials* 34, 4703–4713. doi: 10.1016/j.biomaterials.2013.03.007
- Schroeder, K. E., and Chestek, C. A. (2016). Intracortical brain-machine interfaces advance sensorimotor neuroscience. *Front. Neurosci.* 10:291. doi: 10.3389/fnins.2016.00291
- Schwartz, A. B. (2004). Cortical neural prosthetics. *Annu. Rev. Neurosci.* 27, 487–507.
- Schwartz, A. B., Cui, X. T., Weber, D. J., and Moran, D. W. (2006). Brain-controlled interfaces: movement restoration with neural prosthetics. *Neuron* 52, 205–220.
- Shanks, N., Greek, R., and Greek, J. (2009). Are animal models predictive for humans? *Philos. Ethics Human. Med.* 4:2. doi: 10.1186/1747-5341-4-2
- Skousen, J. L., Bridge, M. J., and Tresco, P. A. (2015). A strategy to passively reduce neuroinflammation surrounding devices implanted chronically in brain tissue by manipulating device surface permeability. *Biomaterials* 36, 33–43. doi: 10.1016/j.biomaterials.2014.08.039
- Sridharan, A., Rajan, S. D., and Muthuswamy, J. (2013). Long-term changes in the material properties of brain tissue at the implant–tissue interface. *J. Neural Eng.* 10:066001. doi: 10.1088/1741-2560/10/6/066001
- Subbaroyan, J., Martin, D. C., and Kipke, D. R. (2005). A finite-element model of the mechanical effects of implantable microelectrodes in the cerebral cortex. *J. Neural Eng.* 2, 103–113.
- Usoro, J. O., Shih, E., Black, B. J., Rihani, R. T., Abbott, J., Chakraborty, B., et al. (2019). Chronic stability of local field potentials from standard and modified Blackrock microelectrode arrays implanted in the rat motor cortex. *Biomed. Phys. Eng. Exp.* 5:065017.
- Vetter, R. J., Williams, J. C., Nunamaker, E. A., and Kipke, D. R. (2004). Chronic neural recording using silicon-substrate microelectrode arrays implanted in cerebral cortex. *IEEE Trans. Biomed. Eng.* 51, 896–904.
- Wellman, S. M., Eles, J. R., Ludwig, K. A., Seymour, J. P., Michelson, N. J., Mcfadden, W. E., et al. (2018). A materials roadmap to functional neural interface design. *Adv. Funct. Mater.* 28:1701269. doi: 10.1002/adfm.201701269
- White, J. J., Lin, T., Brown, A. M., Arancillo, M., Lackey, E. P., Stay, T. L., et al. (2016). An optimized surgical approach for obtaining stable extracellular single-unit recordings from the cerebellum of head-fixed behaving mice. *J. Neurosci. Methods* 262, 21–31. doi: 10.1016/j.jneumeth.2016.01.010
- Winslow, B. D., and Tresco, P. A. (2010). Quantitative analysis of the tissue response to chronically implanted microwire electrodes in rat cortex. *Biomaterials* 31, 1558–1567. doi: 10.1016/j.biomaterials.2009.11.049
- Wise, K. D. (2005). Silicon microsystems for neuroscience and neural prostheses. *IEEE Eng. Med. Biol. Mag.* 24, 22–29.
- Wise, K. D., and Angell, J. B. (1975). A low-capacitance multielectrode probe for use in extracellular neurophysiology. *IEEE Trans. Biomed. Eng.* 22, 212–219.
- Won, S. M., Song, E., Zhao, J., Li, J., Rivnay, J., and Rogers, J. A. (2018). Recent advances in materials, devices, and systems for neural interfaces. *Adv. Mater.* 30:1800534.
- Working, P. K. (1988). Male reproductive toxicology: comparison of the human to animal models. *Environ. Health Perspect.* 77, 37–44.
- Xindong, L., McCreery, D. B., Bullara, L. A., and Agnew, W. F. (2006). Evaluation of the stability of intracortical microelectrode arrays. *IEEE Trans. Neural. Syst. Rehabil. Eng.* 14, 91–100.
- Xindong, L., McCreery, D. B., Carter, R. R., Bullara, L. A., Yuen, T. G. H., and Agnew, W. F. (1999). Stability of the interface between neural tissue and chronically implanted intracortical microelectrodes. *IEEE Trans. Rehabil. Eng.* 7, 315–326.
- Yan, G., Zhang, G., Fang, X., Zhang, Y., Li, C., Ling, F., et al. (2011). Genome sequencing and comparison of two nonhuman primate animal models, the cynomolgus and Chinese rhesus macaques. *Nat. Biotechnol.* 29, 1019–1023. doi: 10.1038/nbt.1992
- Zhang, W., Li, Z., Gilles, M., and Wu, D. (2014). Mechanical simulation of neural electrode-brain tissue interface under various micromotion conditions. *J. Med. Biol. Eng.* 34, 386–392.
- Zhong, Y., and Bellamkonda, R. V. (2007). Dexamethasone-coated neural probes elicit attenuated inflammatory response and neuronal loss compared to uncoated neural probes. *Brain Res.* 1148, 15–27.

Conflict of Interest: The authors declare that the research was conducted in the absence of any commercial or financial relationships that could be construed as a potential conflict of interest.

Copyright © 2020 Mahajan, Hermann, Bedell, Sharkins, Chen, Chen, Meade, Smith, Rayyan, Feng, Kim, Schiefer, Taylor, Capadona and Erefej. This is an open-access article distributed under the terms of the Creative Commons Attribution License (CC BY). The use, distribution or reproduction in other forums is permitted, provided the original author(s) and the copyright owner(s) are credited and that the original publication in this journal is cited, in accordance with accepted academic practice. No use, distribution or reproduction is permitted which does not comply with these terms.